Theor. Appl. Climatol. (2008) 94: 13–24
DOI 10.1007/s00704-007-0340-2
Printed in The Netherlands

Theoretical and Applied Climatology

[1] Division of Earth Environmental System, Pusan National University, Busan, Korea
[2] Climate Prediction Center, NCEP/NOAA/NWS, Camp Springs, Maryland, USA

The onset and life span of the Madden–Julian oscillation

K.-H. Seo[1], A. Kumar[2]

With 7 Figures

Received 30 March 2007; Accepted 14 June 2007; Published online 12 October 2007

Summary

While the canonical life cycle of the Madden–Julian oscillation (MJO) is relatively well studied, little attention has been given to the determination of its periodicity and the detailed low-level dynamic structure during the onset phase. Here we present observational evidence of significant dynamical linkage between MJO convection and life span of MJO events. It is revealed that over the Indian Ocean, the low-level moisture convergence (LLMC) induced by easterly zonal wind anomaly and equatorward converging meridional wind anomaly preconditions about 3–5 days prior to the development of onset convection. Further, it is explicitly shown that the stronger LLMC tends to induce more intense MJO convection in the Indian Ocean, indicating that the LLMC paradigm is effectively operative in the initiation of MJO convection. The results show that the life span of the MJO is determined by the strength of the convective coupling with the large-scale circulation. That is, stronger MJO convection exhibits a longer life span due to stronger coupling between the tropical convection and circulation, and hence the slower eastward propagation of low-level circulation. In contrast, the weak MJO events favor a short period of the cycle and bear a similarity to the convectively coupled equatorial Kelvin waves. Thus, the greater LLMC tends to induce the greater MJO convection, which in turn gives rise to the strong coupling with lower-level circulation and propagating slowly to the east. The linear relationship between the convection strength and life span is shown to be greater in boreal winter.

Correspondence: Dr. Kyong-Hwan Seo, Division of Earth Environmental System, Atmospheric Science Major, Pusan National University, Busan, Korea, e-mail: khseo@pusan.ac.kr

1. Introduction

The Madden–Julian oscillation (MJO) is the most prominent mode of intraseasonal variability in the tropics on the time scales of 30–70 days (Madden and Julian 1994; Zhang 2005). Recent observational and modeling studies stress the importance of air–sea interaction and anomalous or basic state sea surface temperature (SST) in the development and propagation of the MJO (Krishnamurti et al. 1988; Flatau et al. 1997; Sperber et al. 1997; Waliser et al. 1999; Woolnough et al. 2000; Kemball-Cook and Wang 2001; Inness et al. 2003; Fu and Wang 2004; Seo et al. 2007). The MJO directly affects the climate of tropical atmosphere and ocean. For example, intraseasonal patterns of cloudiness and rainfall are more pronounced over the Eastern Hemisphere than in the Western Hemisphere. The coherent fluctuations of SST, heat fluxes and radiation fluxes at sea surface appear along with the passage of MJO convective events (Woolnough et al. 2000; Kemball-Cook and Wang 2001). It is of special interest that a series of westerly wind bursts over the Pacific warm pool associated with an MJO event intensified the development of the 1997–1998 and 2002–2003 El Niño events by generating strong downwelling equatorial Kelvin waves (McPhaden 1999, 2004; Seo and Xue 2005).

Tropical convective activity also influences the extratropical regions through the interaction

between MJO convective forcing and large-scale circulation (e.g. Fig. 1 in Lin et al. 2005). The evolution and propagation of MJO convection have been shown to develop the persistent North Pacific circulation anomalies and extreme precipitation events along the western United States during boreal winter (e.g. Weickmann 1983; Liebmann and Hartmann 1984; Lau and Philips 1986; Higgins and Schubert 1996; Mo and Higgins 1998; Jones 2000). Accordingly a proper representation of the tropical convective forcing is likely to enhance extended-range weather forecast skill in the extratropics (Ferranti et al. 1990). Furthermore, its influence is also strongly linked to the Asian summer monsoon (Lau and Chan 1986; Annamalai and Slingo 2001). The active and break cycle of the monsoon is significantly related to the northwestward propagation of intraseasonal convective anomaly toward the Indian subcontinent (Krishnan et al. 2000; Annamalai and Slingo 2001).

A number of fundamental questions need to be clearly resolved concerning the initiation, propagation and periodicity of MJO events. For example, much of the observational and modeling work has been devoted to the studies on the canonical life cycle of the MJO (e.g. Hendon and Salby 1994; Salby et al. 1994; Wang and Li 1994), yet relatively few papers have focused on the initiation of the MJO (Kemball-Cook and Weare 2001; Seo and Kim 2003) and convective coupling process with circulation, which will impact the life span of the individual cycle. Among the initiation mechanisms, the circumnavigation of the globe by upper-level circulation anomaly emitted from the previous cycle of the MJO has been suggested as a tropical triggering mechanism by several authors (e.g. Knutson et al. 1986; Bladé and Hartmann 1993). Also, an observational case study suggests that upper-level Rossby wave trains propagating into the tropical Indian Ocean region from the extratropics induce vertical motion and onset convection (Hsu et al. 1990). It has been recognized that the onset process by upper-level disturbances is hard to justify due to lack of connecting physical mechanism, although the latter mechanism may act as stochastic forcing as pointed out by Kemball-Cook and Weare (2001).

Instead, the frictional wave-CISK (conditional instability of the second kind), which is one of the currently prevailing paradigms for the development of the MJO, focuses on the low-level process. Jones and Weare (1996) observed that the low-level moisture convergence contributes to the development of onset convection. Especially, Seo and Kim (2003) showed that both Kelvin and Rossby waves play a role in forming low-level moist convergence prior to the onset of the oscillation in the western Indian Ocean. They have shown that the Kelvin waves have encircled from a region of enhanced convection of previous cycle and the Rossby waves are trailing anticyclones of wave response to the reduced convection over the Indian Ocean.

Along with the low-level moisture convergence paradigm, another prevailing view is a discharge-recharge hypothesis put forward by Bladé and Hartmann (1993). They argued that the local oscillation between the discharge and buildup of convective instability determines the onset and period of MJO events. Kemball-Cook and Weare (2001) lent support to this hypothesis by showing the buildup of low-level moist static energy preceding the initiation of MJO convection from the analysis of the radiosonde soundings of the Comprehensive Aerological Reference Data Set.

Recently, Sperber (2003) also stressed the importance of Kelvin and Rossby wave interaction in MJO onset. He showed that enhanced low-level moisture and convergence from the surface to 850 hPa occur in phase with enhanced rainfall in the western Indian Ocean during the onset of the MJO, suggesting the need to look at in detail the temporal and spatial structures of the MJO during the onset stage. In addition, the periodicity of the MJO has not been studied sufficiently. Even if the individual MJO events are expected to exhibit complicated evolution pattern and life span, the factors that affect the period of the MJO should be examined. It will be shown later that this is related to the coupling between MJO convection and large-scale circulation and their propagation.

The purpose of this study is to re-examine the onset mechanism of the MJO and investigate the difference in the propagation characteristics in the intensity of MJO convection. The following questions are addressed below.

1) What are the spatial structures of the dynamic and thermodynamic variables at the onset of the MJO? Is that associated with easterly or westerly zonal wind anomaly?

2) Is there any explicit relationship between low-level moisture convergence and amplitude of the MJO, and between life span and MJO strength?
3) What is different in the propagation of convection and large-scale circulation for strong and weak MJO events?

To address these issues, composite maps and scatter diagrams will be analyzed on proxy data for deep convection and atmospheric variables in the tropics. Data sets and analysis variables used in the study are introduced in Sect. 2. Section 3 describes compositing method based on the variation of OLR anomaly over the Indian Ocean. The evolution of convection anomalies and low-level variables will be examined to address the onset process in Sect. 4. Summary and discussion are given in Sect. 5.

2. Data

The observed relationships between tropical convection and atmospheric variables are presented using two main datasets. To represent deep tropical convection, daily mean OLR from the advanced very high resolution radiometer onboard the National Oceanic and Atmospheric Administration (NOAA) polar-orbiting satellites is used (Liebmann and Smith 1996). The OLR dataset interpolated on a $2.5^\circ \times 2.5^\circ$ grid is used for 23-yr period from 1981 to 2003.

Daily zonal and meridional winds, latent heat flux, SLP, and moisture fields have been derived from the National Centers for Environmental Prediction-National Center for Atmospheric Research (NCEP-NCAR) reanalysis (Kalnay et al. 1996) for the same period 1981–2003. The reanalysis data are available on the same 2.5° grid as the OLR data. Using this, the vertically integrated low-level moisture convergence (hereafter LLMC) is calculated as

$$\mathrm{LLMC} = \frac{1}{g}\int_{P_s}^{P_1} \nabla(qV)\, dP, \qquad (1)$$

where q is specific humidity, V is horizontal winds, and g is gravity. LLMC is vertically integrated from 1000 hPa (P_s) to 700 hPa (P_1). Moist static energy is also calculated as $h = C_pT + Lq + gz$, where C_p is the specific heat of air, T air temperature, L latent heat of condensation, q specific humidity, g gravity, and z geopotential height.

Anomaly field of each variable is derived by first removing the smooth annual cycle which contains the time mean and first three annual harmonics at each grid point. Then to capture the 20–100-day variations, Lanczos filter (Duchon 1979) with 141 weights is applied to anomaly fields for all variables used in this study. Extended boreal winter is defined to be the months of November through April and extended boreal summer season is the months of May through October. Throughout the paper, winter (or summer) means extended boreal winter (or extended boreal summer).

3. Methods

To extract the MJO signals, we construct composite maps for convective anomaly and atmospheric variables. The compositing technique employed here is similar to that of Kemball-Cook and Wang (2001). That is, the composite is based on the convective signal as measured by the average OLR anomaly over the Indian Ocean. Individual MJO events are identified by applying the following criteria as shown in Fig. 1: 1) the minimum value of the filtered OLR anomaly averaged over the boxed base region of [65–85° E, 5° S–5° N] is less than $-20\,\mathrm{W\,m^{-2}}$ for boreal winter and $-15\,\mathrm{W\,m^{-2}}$ for boreal summer, and 2) as the MJO event passes through this base region, the box-averaged OLR anomaly should undergo a minimum during the cycle. The cases selected by the above provide the composites for strong MJO events. The Indian Ocean base region is chosen because it is within the region that the largest MJO-related variance appears (e.g. Fig. 3 in Seo et al. 2005). The use of different threshold value stems from a stronger MJO intensity in winter season compared to summer season. The latter is applied to select only MJO events that exhibit the maximum intensity over the Indian Ocean, enhancing onset and propagation signals around the region. The MJO events selected in this way are independent and all composites are centered in time around the day on which the box-averaged OLR is at a minimum. To distinguish significant signals, a student t-test is applied to the composite fields. Preliminary tests show that a reasonable change in OLR

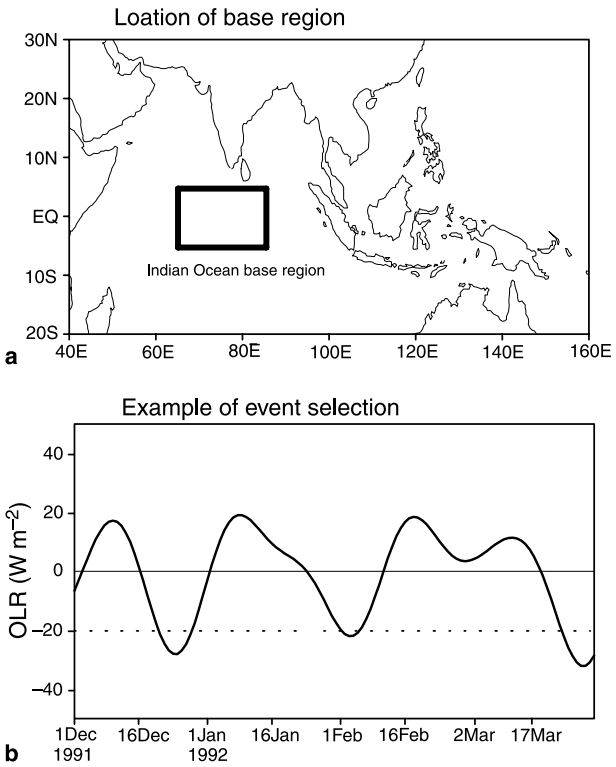

Fig. 1. Compositing procedure: (**a**) location of Indian base region used to form the composites, where OLR ($W\,m^{-2}$) anomalies are averaged; (**b**) example of event selection showing the time series of averaged OLR anomalies for Dec 1992–Mar 1992. The OLR anomalies have been bandpassed through Lanczos filter to give 20–100-day variations. The dotted line denotes the OLR intensity threshold ($-20\,W\,m^{-2}$) for boreal winter season. In this period, three distinct MJO events are selected. The composite is centered in time around the day on which the box-averaged OLR anomaly reaches its minimum value

threshold and base domain does not significantly change the main results.

The time series averaged over the above Indian base region for OLR and LLMC anomalies are used to construct scatter diagrams that show explicit relationships among the intensity of MJO convection and magnitude of LLMC, and life span of the MJO. For the scatter diagrams, whole time series are considered so MJO events of moderate and strong amplitudes are selected. And to evaluate statistical significance, we applied a Monte Carlo test as well as a *t*-test. The former is simulated with 2000 number of trials by scrambling the time series with random number generator and calculating correlation coefficients. The resulting standard deviation (σ) of correlation coefficients provides a critical limit of the null hypothesis of zero correlation. In this study, significance is assessed relative to 95% confidence level corresponding $\pm 1.96\sigma$ levels.

4. Results

4.1 Onset of the MJO

Figure 2 shows the 5° N–5° S – averaged longitude-time lag composite plots of OLR and other variables for boreal winter season. Again zero time lag represents the time when the convective activity in the Indian Ocean base region undergoes the maximum intensity. OLR exhibits the dominant eastward propagation and all other variables also propagate eastward in conjunction with OLR. The appearance of the region of enhanced convection around 50°–65° E at day −15 signifies the beginning of the new cycle of MJO convection. The MJO convection tends to linger for a few days near the maritime continent and redevelops over the western Pacific Ocean. It eventually disappears over the colder SST region of the Western Hemisphere. SLP appears to be strongly coupled with MJO convective forcing over the Indian Ocean but its eastward propagation occurs faster than OLR. It is noticed that negative SLP anomaly arrives at 60° E at day −22, a week earlier than the onset of the MJO convection. More detailed behavior of the SLP propagation will be discussed later.

In Fig. 2b, LLMC appears to lead the OLR by 3–10 days throughout the cycle. At 60° E in the Indian Ocean, LLMC preconditions about 3–5 days before the onset process begins. A careful examination of 1000-hPa specific humidity field (Fig. 2c) reveals that the positive moisture anom-

Fig. 2. Longitude-time composite plots of the 5° S–5° N-averaged 20–100-day bandpass-filtered OLR ($W\,m^{-2}$; colors) and atmospheric variables (contours) during the extended northern winter. (**a**) SLP (interval 12 Pa), (**b**) LLMC (interval $1\,kg\,m^{-2}\,day^{-1}$), (**c**) 1000-hPa specific humidity (interval $0.0001\,kg\,kg^{-1}$), (**d**) 1000-hPa moist static energy (interval $200\,J\,kg^{-1}$), (**e**) 1000-hPa zonal winds (interval of $0.2\,m\,s^{-1}$), and (**f**) latent heat flux (interval $4\,W\,m^{-2}$; positive upward represents evaporative cooling of the surface). All contours except zero lines and all colors are statistically significant at the 95% confidence level

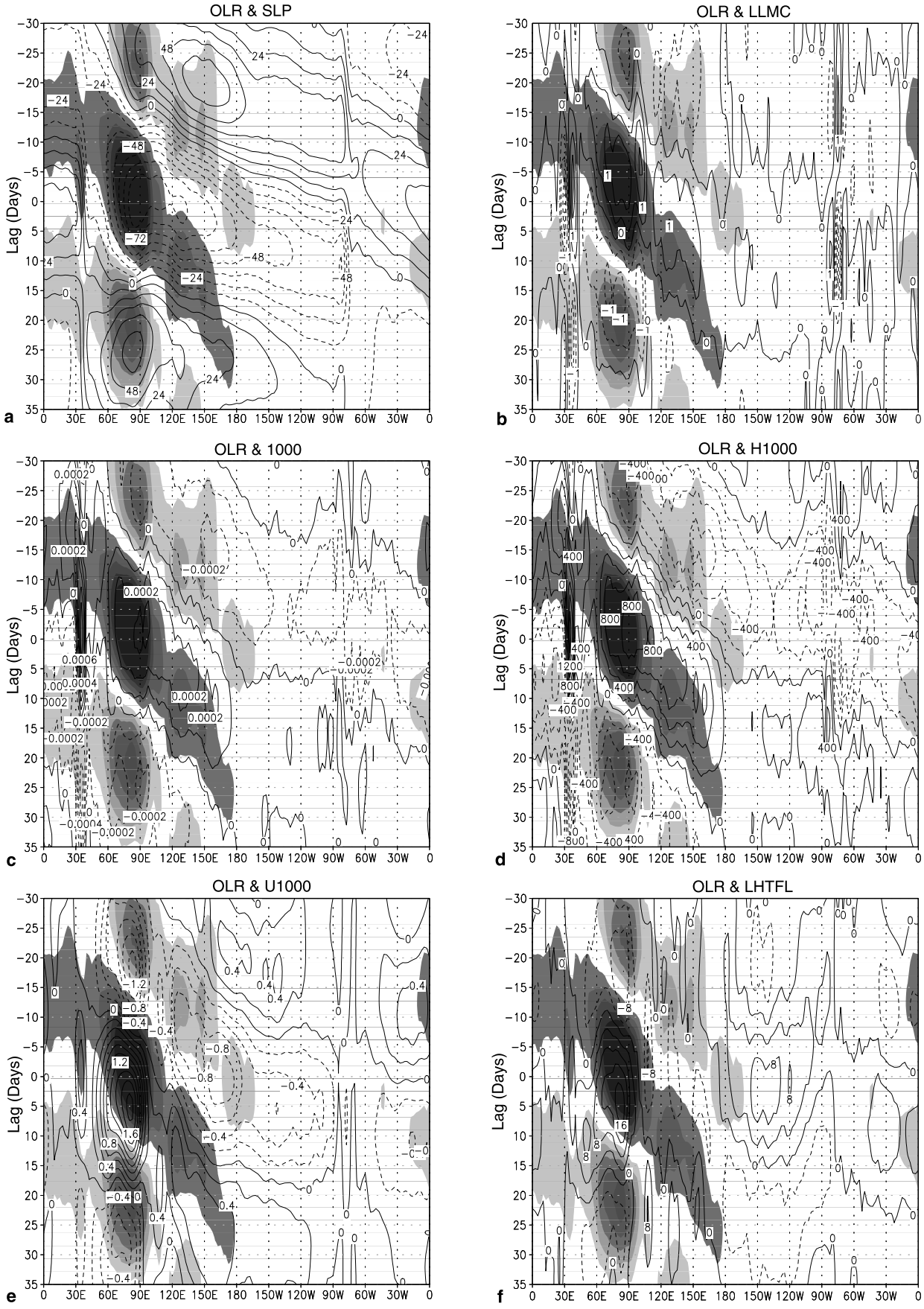
OLR & SLP
OLR & LLMC
OLR & 1000
OLR & H1000
OLR & U1000
OLR & LHTFL
Lag (Days)
a
b
c
d
e
f
−20 −16 −12 −8 −4 4 8 12 16 20

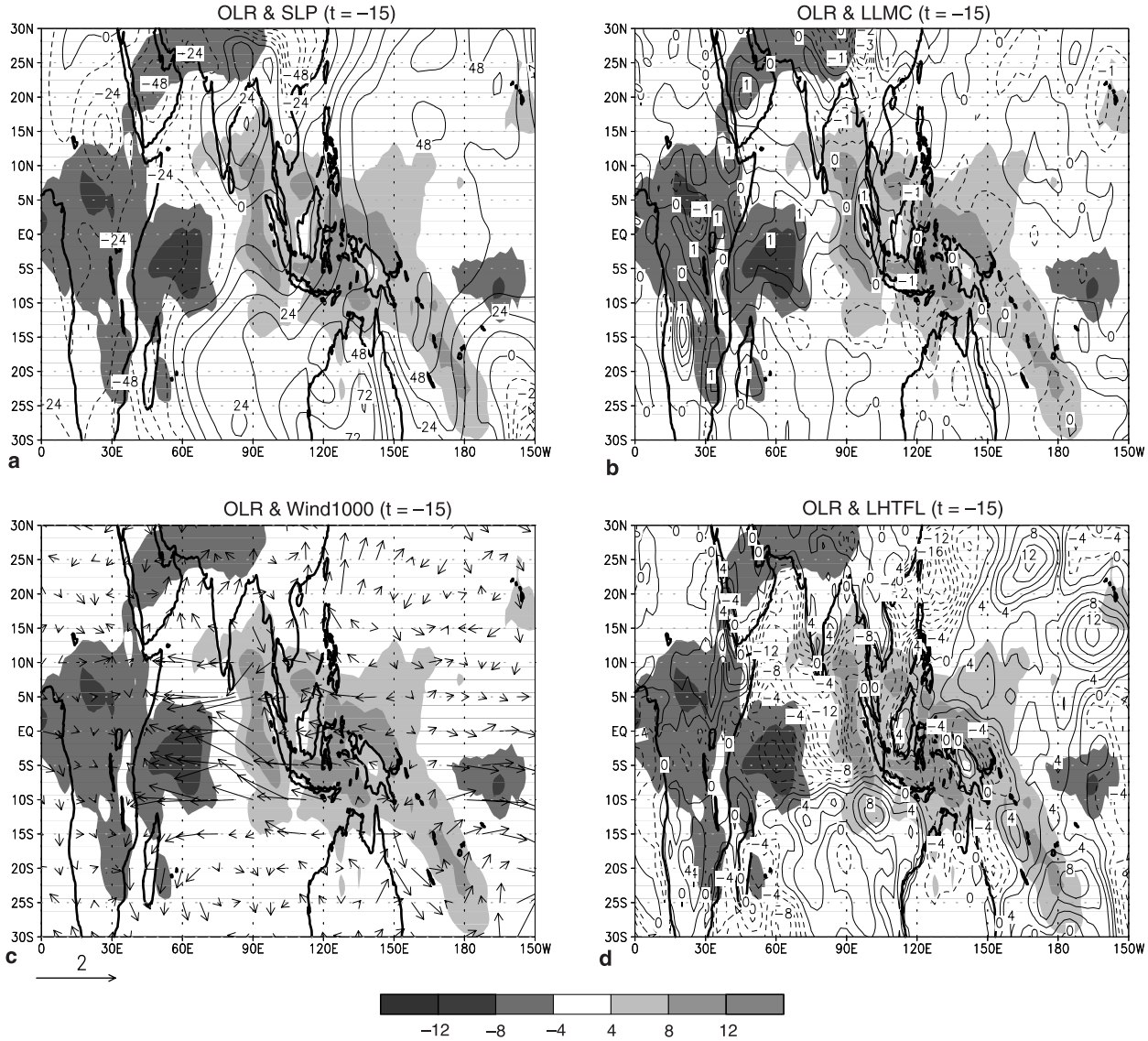

Fig. 3. Composite plots at day −15 for bandpass-filtered OLR (colored) and (**a**) SLP, (**b**) LLMC, (**c**) 1000-hPa horizontal wind vectors, and (**d**) latent heat flux anomalies during the extended northern winter

alies develop near 60° E a few days earlier than the negative OLR anomaly. Likewise, moist static energy (Fig. 2d) also precedes the appearance of the active phase of MJO convection since specific humidity contributes most to the variation of moist static stability (h) as in Kemball-Cook and Weare (2001). In the 1000-hPa zonal wind field (Fig. 2e), easterly winds develop over the Indian Ocean, affecting the onset process at day −15 (see also Fig. 3c). Once MJO convection developed, westerly zonal wind anomaly develops in the Indian Ocean. The progression of latent heat flux (Fig. 2f) is very closely related to the zonal wind field. Because climatological zonal winds over the warm pools are westerlies (not shown), easterly wind anomalies tend to reduce evaporation and westerly anomalies to enhance evaporation. From this, moisture required to increase static energy and generate a new cycle of MJO convection does not come from the latent heat flux variation but from the advective process. Instead, the latent heat flux variation follows the moisture variation as consistent with the result of Weare (2003).

The spatial structures for the variables associated with MJO onset are presented in Fig. 3. At day −15, negative SLP anomalies over the Indian Ocean clearly exhibit Kelvin wave signature (Fig. 3a). The downstream bulge propagates into the region of the reduced convection. To the east

of the enhanced convection (∼85° E), Rossby waves are also seen in the off-equatorial regions in relation to the dynamical response to the suppressed convection. The pressure distribution produced by the Kelvin wave surge and Rossby wave response leads to the formation of easterly wind anomalies, which appear over the entire tropical Indian Ocean (Fig. 3c). Figure 3b shows that low-level moisture convergence over the Indian Ocean leads the convection by about 20°–30° longitude. This moisture convergence is related to the low-level wind variation as in Fig. 3c, which shows strong easterly zonal wind signal and equatorward converging wind over the entire Indian Ocean. So both the frictional zonal wind convergence and equatorward meridional wind convergence lead to the convergence of moisture. As stated above, the climatological circulation in the warm Indian Ocean is westerlies so that easterly anomaly induces the downward negative latent heat flux (Fig. 3d). The reduced evaporation is also evident near 100° E, in the western part of the suppressed convection. Hence, the onset occurs in a westerly basic state, with the easterly anomaly associated with the appearance of the negative SLP anomaly and lower-tropospheric trailing anticyclones of the Rossby wave response (e.g. Matthews 2000; Seo and Kim 2003; Sperber 2003; Seo et al. 2005).

The results show the importance of SLP propagation and pressure distribution and thereby LLMC during the onset phase of MJO convection for strong MJO events. If LLMC is indeed a major factor for the development of MJO convection, then strong LLMC should induce intense MJO convection over the Indian Ocean. To investigate this in a more explicit way, the time series of LLMC and OLR anomalies averaged over the Indian Ocean base box are extracted and all MJO events are taken into account for entire seasons. It is observed that OLR minima appear, in general, within 1–15 days after LLMC peaks. So the scatter diagrams are plotted for the intensity of the convection peak occurring 1–15 days after the appearance of LLMC peak for winter, summer and all seasons (Fig. 4). Around 80 independent cases are selected for each season. A gross feature is that the intensity of MJO convection over the Indian Ocean increases largely linearly with the magnitude of LLMC for both winter and summer seasons, and for whole season. The esti-

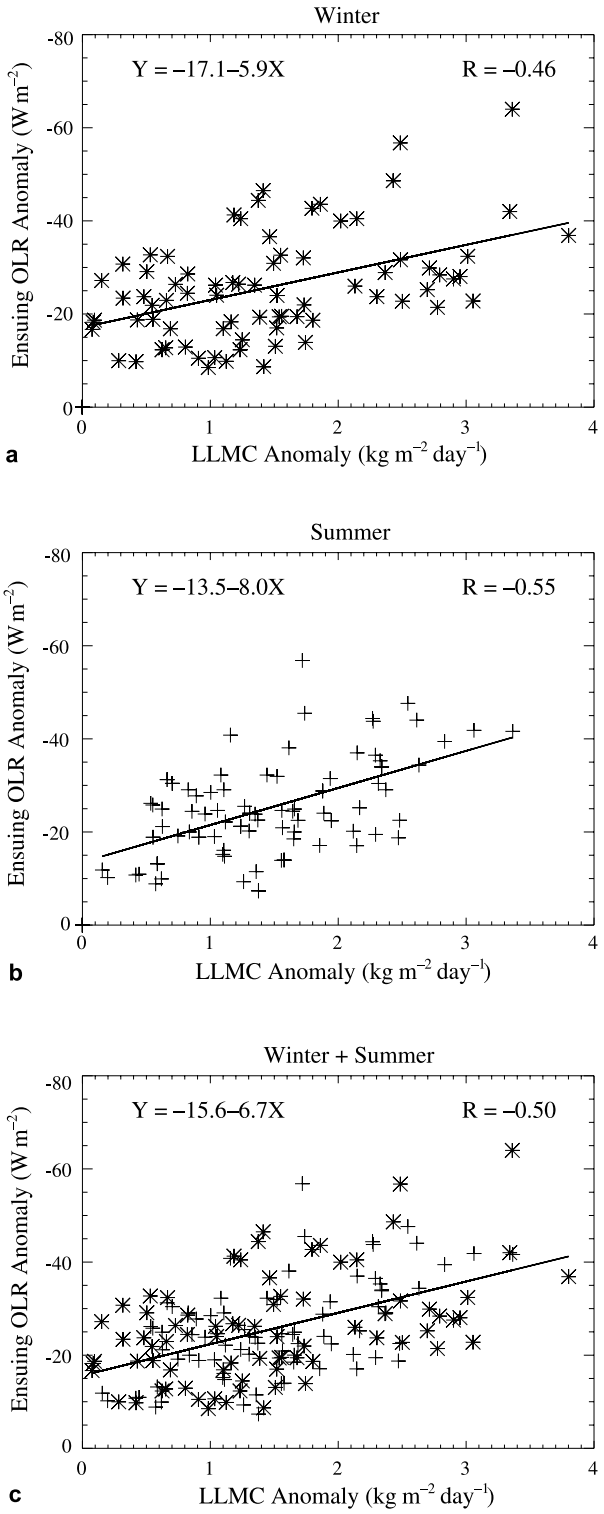

Fig. 4. Scatter diagram of LLMC anomaly (kg m^{-2} day^{-1}) and ensuing OLR anomaly (W m^{-2}) for (**a**) extended winter, (**b**) extended summer, and (**c**) extended winter + summer. The linear line is the best regression line for the data. The correlation coefficient between the two variables is also shown in the plot. The time series is extracted over the average value over the Indian Ocean base box. Asterisk (plus sign) denotes winter (summer) events

mated correlation during the wintertime is 0.46. For summertime case, the low-level moisture convergence explains about 30% of the variance, suggesting that the preconditioning and moisture convergence play an important role also in the onset of the summertime intraseasonal oscillation over the Indian Ocean. Both the *t*-test and Monte Carlo test for the linear regression show that these relationships for both winter and summer and whole seasons are statistically significant at the 95% level [critical correlations for *t*-test (Monte Carlo) are 0.22 (0.23) for winter and summer and 0.16 (0.16) for all seasons]. It should be mentioned that several previous studies have showed the LLMC preceding the occurrence of strong convection in the Indian Ocean (e.g. Jones and Weare 1996; Kemball-Cook and Weare 2001; Seo and Kim 2003), but this study presents the more detailed spatial feature during the onset of the MJO. In particular, the relationship between the preceding LLMC magnitude and the intensity of ensuing MJO convection has been presented in an explicit manner. This information can be used for improving prediction skill of the MJO from dynamical and empirical forecast models.

4.2 Life span of the MJO

The relationships between the intensity and life span of MJO convection for northern extended winter, summer and all seasons are shown in Fig. 5. The life span of MJO convection is estimated as a time interval between two successive minima of the OLR time series averaged over the Indian Ocean base box. The diagram includes only enhanced convection events and the basic property for suppressed convection events is nearly identical to the enhanced convection events. It is evident that the life span of individual events is approximately linearly proportional to the magnitude of OLR anomalies over the Indian Ocean during both seasons. But northern winter season has a higher degree of linear approximation (more than 1.5 times the summertime correlation) presumably due to stronger eastward propagating MJO signals in boreal wintertime. It explains about 34% of the variance of the enhanced convection strength over the Indian Ocean. Also it shows a steeper slope of regression line than the summer counterpart. The candidate reasons for this difference may include the complex propagation and rather weaker convection signal associated with the boreal summer intraseasonal oscillation. For the whole seasons, the correlation coefficient between the current

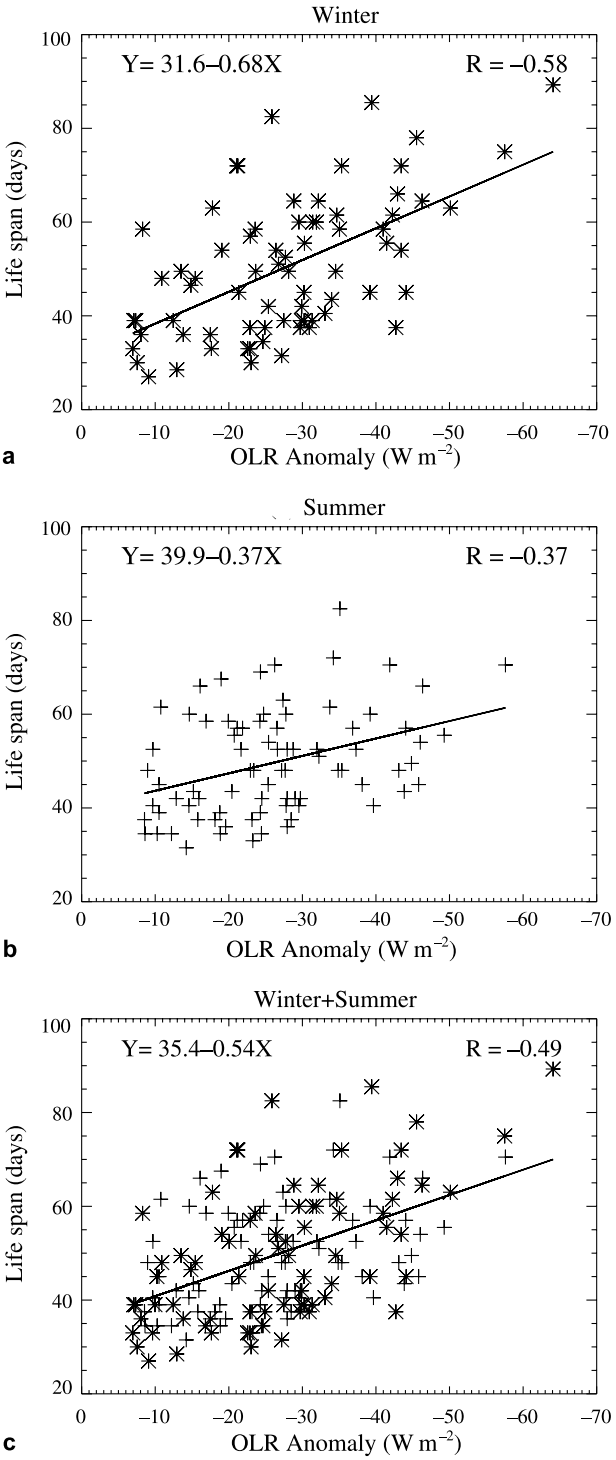

Fig. 5. Scatter diagram between the intensity and period of OLR anomalies for (**a**) extended winter, (**b**) extended summer, and (**c**) extended winter + summer. The linear line is the best regression line for the data. The correlation coefficient between the two variables is also shown in the plot. Asterisk (plus sign) denotes winter (summer) events

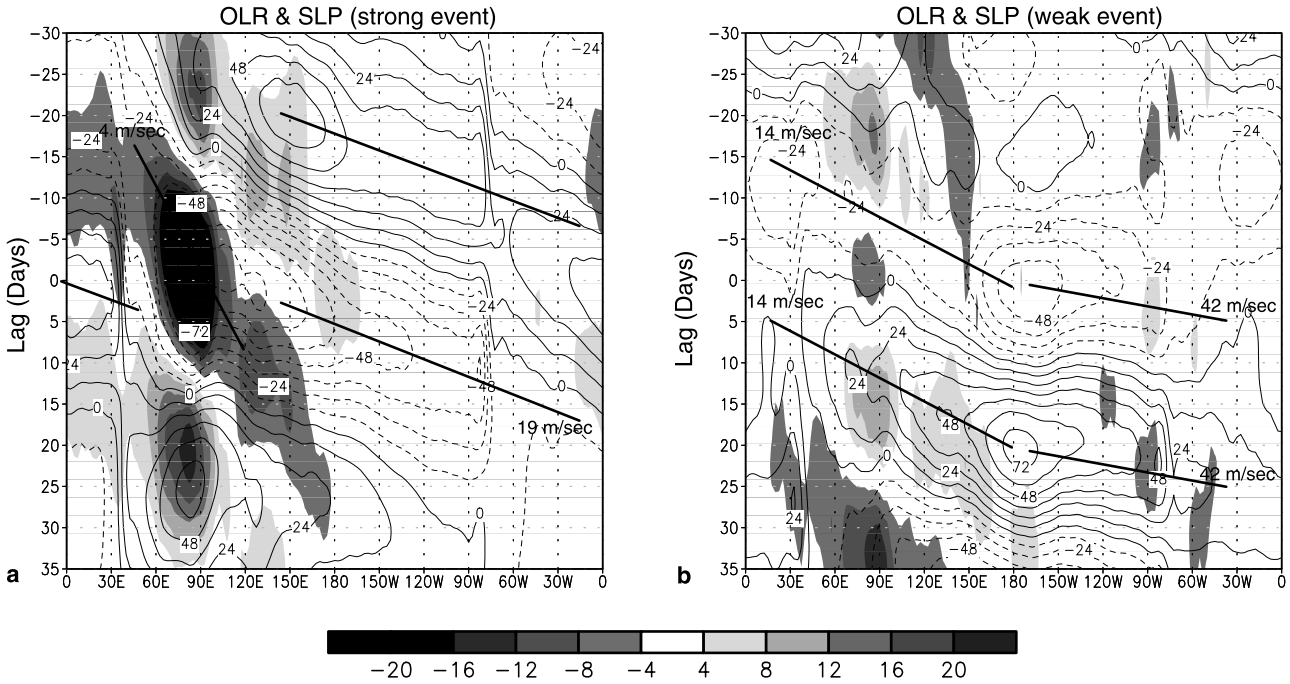

Fig. 6. Longitude-time composite plot of the 5° S–5° N-averaged bandpass-filtered OLR ($W\,m^{-2}$; color) and SLP (contoured at intervals of 12 Pa) for (**a**) strong, and (**b**) weak convection events during the northern extended winter. Thick lines denote the approximate propagation speed of SLP

MJO strength and life span is ∼0.5. Importantly, the slopes of the regression lines are all significantly different from zero at the 95% confidence level measured by the *t* and Monte Carlo tests. That is, intense convection events over the Indian Ocean tend to give rise to a longer period of the cycle, whereas weak convection events there are likely to result in a shorter cycle of the MJO. This relationship also holds in the separate seasons.

To examine a possible reason for this significant relationship, we speculate that this is regulated in part through the coupling process between the MJO convection and the large-scale circulation. For this, the composites of convection and SLP for strong MJO events (Fig. 6a; which is copied from Fig. 2a) are compared to the weak events (Fig. 6b) defined as cases with the box-averaged OLR $\leq |-10\,W\,m^{-2}|$ over the Indian Ocean. Fig. 6a (same as Fig. 2a) shows two-regime structures in the propagation of SLP. In the warm pool regions where the circulation is strongly coupled with convection, the SLP signal propagate at about the same speed of $\sim 4\,m\,s^{-1}$ as the convection and the wave is characterized by smaller equivalent depths (Wheeler et al. 2000), but in the Western Hemisphere, the SLP decouples from the weakening convection, propagating as a free Kelvin wave with much faster phase speed of $\sim 19\,m\,s^{-1}$ (see also Hendon and Salby 1994). The mean period based on the reappearance of enhanced convections or suppressed convection in the Indian Ocean is ∼45 days.

The composite plot for weak MJO convection events during the northern winter is shown in Fig. 6b. The 24 independent events are selected. In this case, the MJO convection shows much smaller longitudinal displacement compared to the strong case and decays very fast, resulting in the period of ∼33 days for MJO convection. With this short life span, SLP also propagates faster than the strong case. The propagation speed of SLP over the warm pool waters amounts to $\sim 14\,m\,s^{-1}$, more than three times the speed of SLP for the strong case. In the Western Hemisphere, there appears the convection free region and SLP propagates at a speed of $\sim 42\,m\,s^{-1}$, twice as fast as it does in the development region of MJO convection. In fact, this faster propagation resembles the characteristics of the convectively coupled equatorial Kelvin wave presented in Wheeler et al. (2000). Such a similar propagation speed appears because according to their plot of wavenumber-frequency spectra for OLR and theoretically derived equatorial wave dispersion curves, a portion of MJO variance overlaps the region of the convectively coupled Kelvin

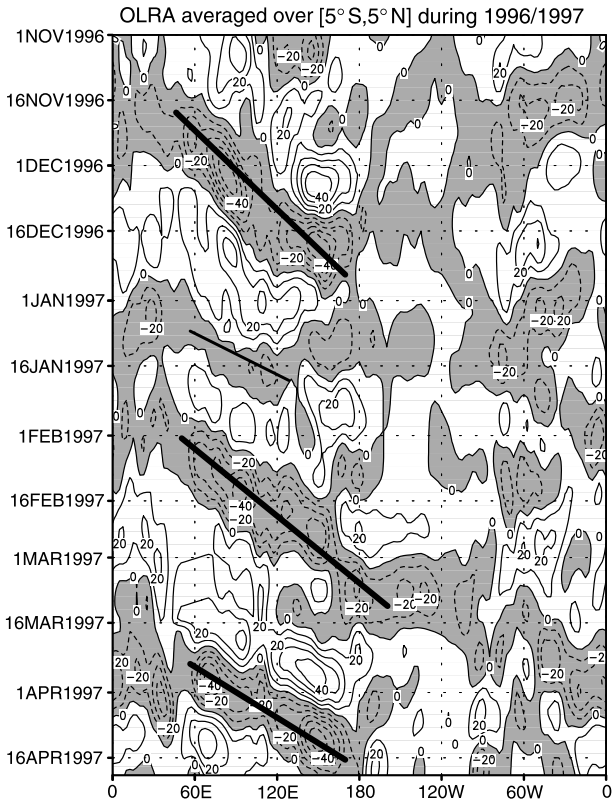

Fig. 7. Propagation of OLR anomalies averaged over [5° S–5° N] during 1996/97 winter. Enhanced convection (negative OLR) regions are shaded. Solid lines denote the approximate propagation of OLR anomalies for strong (*thick*) and weak (*thin*) events

wave at its longer period. Figure 6 also shows that MJO events that have more negative OLR last longer and exhibit greater longitudinal displacements, being consistent with the recent work of Jones et al. (2004; their Fig. 7). The strong and weak composites (using $\mathrm{OLR} \geq |-15\,\mathrm{W\,m^{-2}}|$ and $\mathrm{OLR} \leq |-10\,\mathrm{W\,m^{-2}}|$, respectively) during the summer season (not shown) provide remarkably identical pictures for the evolution of OLR and SLP to the winter counterparts.

This dependence of MJO life span on SLP propagation indicates that when MJO convection is weak, the convective constraint on the propagation of the large-scale circulation becomes weak. Accordingly, SLP propagates east much faster than that of stronger events, and hence, resulting in a short cycle. Therefore, the life span of the MJO is set by the time needed for SLP anomaly to travel east as a convectively coupled signal over the warm pools, and to propagate as a dry free Kelvin wave.

5. Summary

Onset mechanism of the MJO and dynamical coupling structures between MJO convection and large-scale circulation are investigated using the composite analysis and scatter diagrams for the 21 years of the daily reanalysis and OLR data. It is seen that over the Indian Ocean, low-level moisture convergence (LLMC) preconditions about 3–5 days before onset convection develops. The increase in the LLMC and moist static energy is induced by easterly wind anomalies and equatorward converging meridional wind anomalies so the frictional wave-CISK mechanism is operative during the onset of the new MJO event. There exists a statistically significant relationship between the intensity of OLR and LLMC, indicating that stronger LLMC tends to induce more intense MJO convection over the Indian Ocean. It should be noted that the relationship between the LLMC and convection intensity can improve the forecast skill of the MJO over the Indian Ocean during the onset stage from dynamical and statistical models since the forecast skill of weak or null initial condition has been shown to be significantly smaller than the strong initial conditions (e.g. Seo et al. 2005).

An important finding from the time series of OLR averaged over the Indian Ocean is that the intense convection events there tend to give rise to a longer cycle of the MJO, whereas the weak convection events result in a shorter period of the cycle. It is speculated that this statistically significant relation is mainly from dynamical coupling between MJO convection and propagating large-scale low-level circulation. To show this, the composites for OLR and SLP anomalies are constructed for strong and weak MJO events. The result indicates that the propagation speed of SLP for weak convection events is more than twice the SLP speed for the strong cases. When MJO convection is weak, convective coupling with the large-scale circulation is weak so that the circulation propagates as a free Kelvin wave much faster than the stronger convection events.

The Madden–Julian oscillation is an oscillation in intensity and period. An interesting example exhibiting the above-mentioned characteristics is shown in the evolution of equatorial OLR anomalies during 1996/97 winter season (Fig. 7). This displays 1) slower (faster) propagation for stron-

ger (weaker) event, 2) longer (shorter) period for stronger (weaker) event, and 3) greater (less) longitudinal displacement for stronger (weaker) event.

Currently, most general circulation models (GCMs) have a difficulty in producing longitudinal propagation across the Maritime Continent for the MJO. Although a recent study suggests that poor representation of the Maritime Continent in GCMs may inhibit MJO events traveling out into the west Pacific (Inness and Slingo 2006), it seems that other factors including background vertical wind shear and convective parameterization also play a role. Correct longitudinal displacements across this region may provide a chance to examine whether atmospheric and coupled GCMs properly simulate the propagation of low-level circulation forced by MJO convective heating and dynamical coupling between MJO convection and circulation. The failure of this will cause incorrect MJO onset and propagation process and its period.

Acknowledgments

The author would like to thank Drs. Kingtse Mo and Yan Xue at Climate Prediction Center/NCEP/NOAA for their valuable comments and suggestions and Dr. Shuntai Zhou for the discussion on the Monte Carlo test. This work was funded by the Korea Meteorological Administration Research and Development Program under Grant CATER 2007-4208.

References

Annamalai H, Slingo JM (2001) Active/break cycles: diagnosis of the intraseasonal variability of the Asian Summer Monsoon. Clim Dyn 18: 85–102

Bladé I, Hartmann D (1993) Tropical intraseasonal oscillations in a simple nonlinear model. J Atmos Sci 50: 2922–2939

Duchon CE (1979) Lanczos filtering in one and two dimensions. J Appl Meteor 18: 1016–1022

Ferranti L, Palmer TN, Molteni F, Klinker E (1990) Tropical-extratropical interaction associated with the 30–60 day oscillation and its impact on medium and extended range prediction. J Atmos Sci 47: 2177–2199

Flatau M, Flatau PJ, Phoebus P, Niiler PP (1997) The feedback between equatorial convection and local radiative and evaporative processes: the implications for intraseasonal oscillations. J Atmos Sci 54: 2373–2340

Fu X, Wang B (2004) The boreal summer intraseasonal oscillation simulated in a hybrid coupled atmosphere-ocean model. Mon Wea Rev 132: 2628–2649

Hendon HH, Salby ML (1994) The life cycle of the Madden–Julian oscillation. J Atmos Sci 51: 2225–2237

Higgins RW, Schubert SD (1996) Simulations of persistent North Pacific circulation anomalies and interhemispheric teleconnections. J Atmos Sci 53: 188–207

Hsu HH, Hoskins BJ, Jin FF (1990) The 1985/1986 intraseasonal oscillation and the role of the extratropics. J Atmos Sci 47: 823–839

Inness PM, Slingo JM (2006) The interaction of the Madden–Julian oscillation with the maritime continent in a GCM. Quart J Roy Meteor Soc 132: 1645–1667

Inness PM, Slingo JM, Guilyardi E, Cole J (2003) Simulation of the Madden–Julian oscillation in a coupled general circulation model. Part II: The role of the basic state. J Climate 16: 365–382

Jones C (2000) Occurrence of extreme precipitation events in California and relationships with the Madden–Julian oscillation. J Climate 13: 3576–3587

Jones C, Weare BC (1996) The role of low-level moisture convergence and ocean latent heat fluxes in the Madden and Julian oscillation: an observational analysis using ISCCP data and ECMWF analyses. J Climate 9: 3086–3104

Jones C, Carvalho LMV, Higgins RW, Waliser DE, Schemm J-KE (2004) Climatology of tropical intraseasonal convective anomalies: 1979–2002. J Climate 17: 523–539

Kalnay E et al (1996) The NCEP/NCAR 40-year reanalysis project. Bull Amer Meteor Soc 77: 437–471

Kemball-Cook S, Weare BC (2001) The onset of convection in the Madden–Julian oscillation. J Climate 14: 780–793

Kemball-Cook S, Wang B (2001) Equatorial waves and air–sea interaction in the boreal summer intraseasonal oscillation. J Climate 14: 2923–2942

Knutson T, Weickmann K, Kutzbach T (1986) Global scale intraseasonal oscillations of outgoing longwave radiation and 250-mb zonal wind. Mon Wea Rev 114: 605–623

Krishnamurti TN, Dosterhof D, Mehta A (1988) Air–sea interaction on the time scale of 30-50 days. J Atmos Sci 45: 1304–1322

Krishnan R, Zhang C, Sugi M (2000) Dynamics of breaks in the Indian summer monsoon. J Atmos Sci 57: 1354–1372

Lau K-M, Chan PH (1986) Aspects of the 40–50 day oscillation during the northern summer as inferred from the outgoing longwave radiation. Mon Wea Rev 114: 1354–1367

Lau K-M, Phillips TJ (1986) Coherent fluctuations of extratropical geopotential height and tropical convection in intraseasonal time scales. J Atmos Sci 43: 1164–1181

Liebmann B, Hartmann DL (1984) An observational study of tropical midlatitude interaction on intraseasonal time scales during winter. J Atmos Sci 41: 3333–3350

Liebmann B, Smith CA (1996) Description of a complete (interpolated) OLR dataset. Bull Amer Meteor Soc 77: 1275–1277

Lin JL et al (2005) Tropical intraseasonal variability in 14 IPCC AR4 climate models: Part I: Convective signals. J Climate 19: 2665–2690

Madden RA, Julian PR (1994) Observations of the 40–50-day tropical oscillation – A review. Mon Wea Rev 122: 814–837

Matthews AJ (2000) Propagation mechanisms for Madden–Julian Oscillation. Quart J Roy Meteor Soc 126: 2637–2651

McPhaden MJ (1999) Genesis and evolution of the 1997–98 El Niño. Science 283: 950–954

McPhaden MJ (2004) Evolution of the 2002/03 El Niño. Bull Amer Meteor Soc 85: 677–695

Mo KC, Higgins RW (1998) Tropical influences on California precipitation. J Climate 11: 412–430

Salby ML, Garcia RR, Hendon HH (1994) Planetary-scale circulations in the presence of climatological and wave-induced heating. J Atmos Sci 51: 2344–2367

Seo K-H, Kim K-Y (2003) Propagation and initiation mechanisms of the Madden–Julian oscillation. J Geophys Res 108: 4384, doi:10.1029/2002JD002876

Seo K-H, Schemm J-KE, Jones C, Moorthi S (2005) Forecast skill of the tropical intraseasonal oscillation in the NCEP GFS dynamical extended range forecasts. Clim Dyn 25: 265–284

Seo K-H, Schemm J-KE, Wang W, Kumar A (2007) The boreal summer intraseasonal oscillation simulated in the NCEP Climate Forecast System (CFS): the effect of sea surface temperature. Mon Wea Rev 135: 1807–1827

Seo K-H, Xue Y (2005) MJO-related oceanic Kelvin waves and the ENSO cycle: a study with the NCEP Global Ocean Data Assimilation. Geophys Res Lett 32: L07712, doi: 10.1029/2005GL022511

Sperber KR (2003) Propagation and the vertical structure of the Madden–Julian oscillation. Mon Wea Rev 131: 3018–3037

Sperber KR, Slingo JM, Inness PM, Lau K-M (1997) On the maintenance and initiation of the intraseasonal oscillation in the NCEP/NCAR reanalysis and in the GLA and UKMO AMIP simulations. Clim Dyn 13: 769–795

Waliser DE, Lau K-M, Kim J-H (1999) The influence of coupled sea surface temperatures on the Madden–Julian Oscillation: a model perturbation experiment. J Atmos Sci 56: 333–358

Wang B, Li T (1994) Convective interaction with boundary-layer dynamics in the development of a tropical intraseasonal system. J Atmos Sci 51: 1386–1400

Weare BC (2003) Composite singular value decomposition analysis of moisture variations associated with the Madden–Julian oscillation. J Climate 16: 3779–3792

Weickmann KM (1983) Intraseasonal circulation and outgoing longwave radiation modes during Northern Hemisphere winter. Mon Wea Rev 111: 1838–1858

Wheeler M, Kiladis GN, Webster PJ (2000) Large-scale dynamical fields associated with convectively coupled equatorial waves. J Atmos Sci 57: 613–640

Woolnough SJ, Slingo JM, Hoskins BJ (2000) The relationship between convection and sea surface temperature on intraseasonal timescales. J Climate 13: 2086–2104

Zhang C (2005) Madden–Julian oscillation. Rev Geophysics 43: RG2003